Chapter 4

SYNTHESIS AND CHARACTERIZATION OF NANOADSORBENTS

In this chapter synthesis and characterization of the selected nano adsorbents i.e. nanocrystalline zirconia and nanocrystalline iron oxide/hydroxide have been discussed. Effect of initial concentration of precursor has been discussed. In case of nanocrystalline zirconia, the effect of temperature on crystallite size was cautiously studied.

4.1. Synthesis of nano crystalline zirconia

Six samples of nano crystalline zirconia were synthesized by precipitation. The precipitation of $ZrOCl_2.8H_2O$ is carried out by ammonia. The precipitation reaction is as follows (Tyagi *et al.* 2006):

$$ZrOCl_2.8H_2O + 2NH_4OH \rightarrow Zr(OH)_4 + NH_4Cl \quad (4.1)$$

The calcination of synthesized zirconium hydroxide led to synthesis of zirconia:

$$Zr(OH)_4 \rightarrow ZrO_2 + H_2O \quad (4.2)$$

The synthesized material was then dried, crushed and sieved. It was then stored in desiccator for further application.

4.2. XRD analysis of nano crystalline zirconia

The X-ray diffraction pattern (Figure 4.1) was used to estimate the crystallite size (Å) of all samples. The crystallite size (Table 4.1) was calculated by using Scherrer's formula (Tyagi *et al.* 2006):

$$\text{Crystallite size} = \frac{K_1 \lambda}{W_1 \cos\theta} \quad (4.3)$$

Where K_1 (0.9) is the shape factor, λ (1.5414 Å) is the wavelength of X-ray used, W_1 is the width (full width at half maxima) of X-ray diffraction peak in radians and θ is Bragg angle.

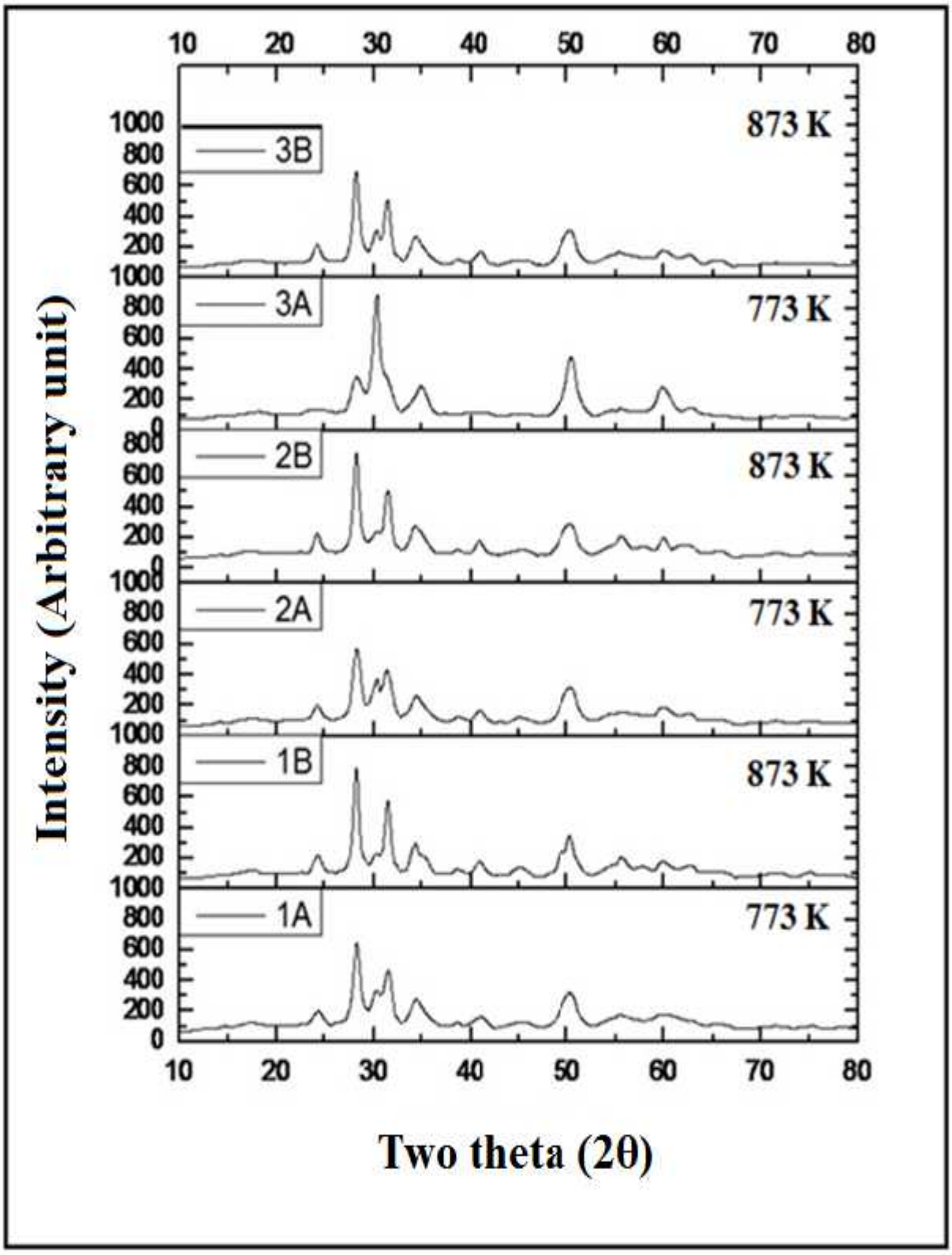

Figure 4.1 XRD of synthesized nano crystalline zirconia samples

Table 4.1 Crystallite size of synthesized nanocrystalline zirconia samples

	Sample code					
	1A	1B	2A	2B	3A	3B
	Calcination temperature					
	773 K	873 K	773 K	873 K	773 K	873 K
2 θ	**Crystallite size (nm)**					
28	16	20.5	13.4	19.2	6.4	17.8
30	7.9	8.3	13.3	10.1	15.6	12.5
31	10.6	21.8	8.5	19.2		15.6
50	6	6.2	6.3	5.7	9.1	5.8
60	2.9	7	7.6	12.1	6.6	7

4.3. Impact of temperature and initial concentration on crystallite size of nano crystalline zirconia

The XRD data of synthesized samples matched at 30.2^{o} (101), 50.2^{o} (112) and 60.2^{o} (211) with JCPDS card number 79-1769 (ICDD 2003) and the peaks at 28.1^{o} ($\overline{1}$ 11), 31.4^{o} (111) matched with JCPDS card number 78-1807 (ICDD 2003). The size of nanocrystalline zirconia lies in the range of 2.9 to 21.8 nm. The rise of temperature diminishes thermodynamically driving force which subsequently causes declination of nucleus density and increase the critical size of the nuclei (Rashidi and Amadeh 2009). Tyagi et al. (2006) expressed an increase in lattice strain with declination of crystallite size. In addition to this, decline in lattice strain occurred with rise of temperature. It also led to rise of crystallite size with the increase of temperature. The nucleation centres increased with increase of precursor concentration. This led to decline in the 'critical size' of nucleating centres. So, crystallite size declines with increase of concentration of precursor.

Sample 1A (0.075 M, calcined at 773K) **Sample 1B (0.075 M, calcined at 873K)**

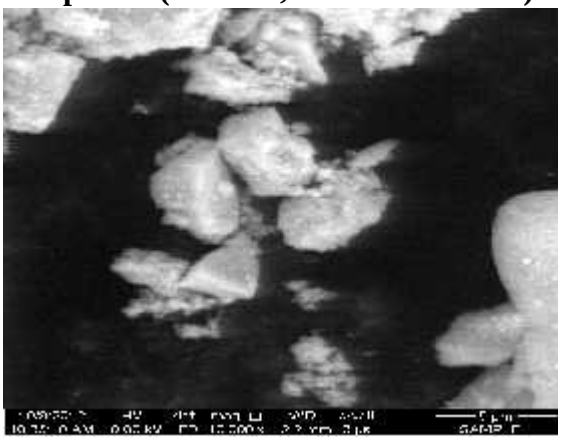

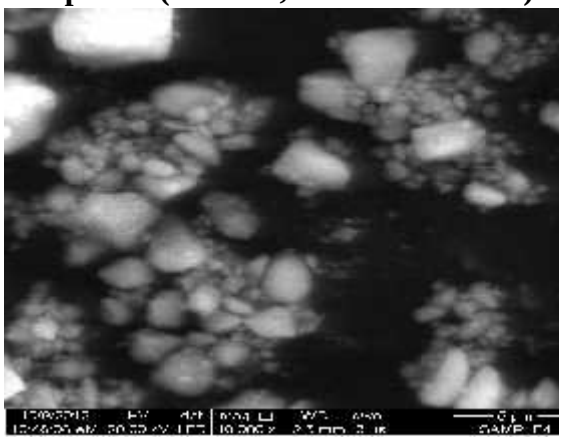

Sample 2A (0.05 M, calcined at 773K) **Sample 2B (0.05 M, calcined at 873K)**

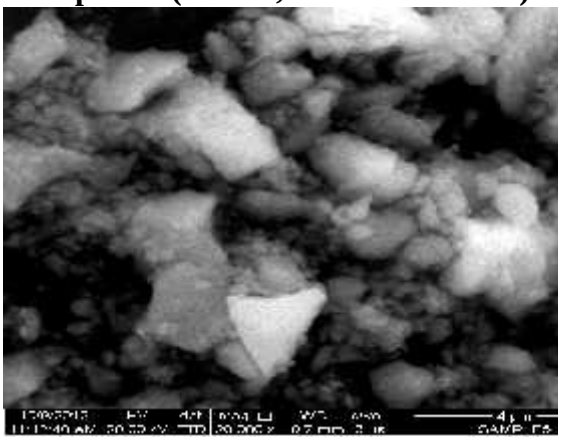

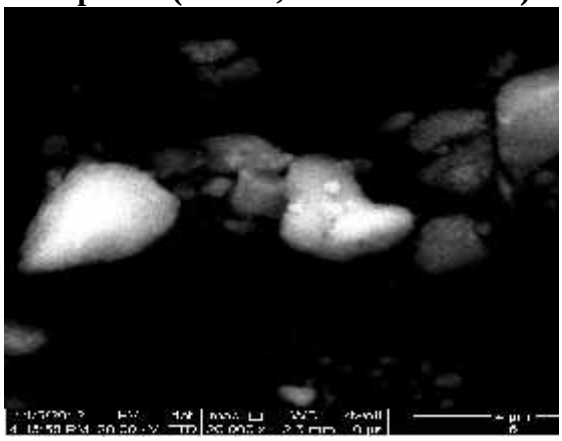

Sample 3A (0.025 M, calcined at 773K) **Sample 3B (0.025 M, calcined at 873K)**

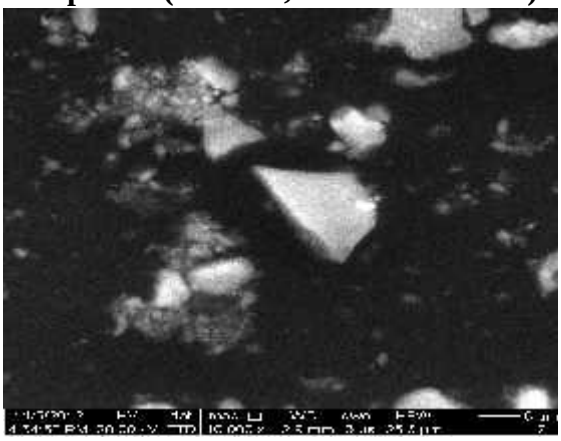

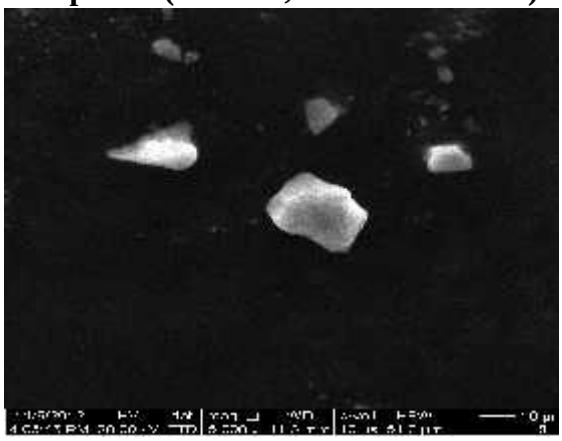

Figure 4.2 SEM of different samples of synthesized nano crystalline zirconia

4.4. SEM analysis of nano crystalline zirconia

Surface morphology of the substance is deciphered by SEM image analysis. The particles were agglomerated, the size of agglomerated particles were 3-5 µm range and irregular in shape. The surface of nanocrystalline zirconia does not show any cracks and its surface is smooth (Figure 4.2). The difference between hydrolysis and condensation, subsequently growth was little due to lack of any co-solvents i.e. ethanol or methanol (Zhang *et al.* 1997), which can act as steric or electrostatic obstacles (Misran *et al.* 2013); the barriers were stabilizes and averted the particles to form agglomerate. In the present system, because of lack of barriers, particles further got hydrolyzed and condensate with other particles and formed agglomerated particles of various sizes owing to their larger surface energy.

4.5. TEM analysis of nano crystalline zirconia

TEM analysis (Figure 4.3 to 4.5) was carried out to analyse the particle size. The nano crystallites were non homogenous and agglomerated. The average particle size increased in all samples with increasing the calcination temperature. The average particle size of samples exists in the domain of 13 nm to 20 nm; excluding sample calcined at 873 K with 0.05 M initial concentration i.e. 35nm. The average particle size determined from TEM was more than what was calculated by XRD analysis. The particle size did not show any significant change with concentration variation (Table 4.2).

Table 4.2 Size variations of different samples based on TEM analysis

Sample	Average size (nm)
1A	13.65
1B	18.39
2A	16.86
2B	31.41
3A	15.94
3B	19.96

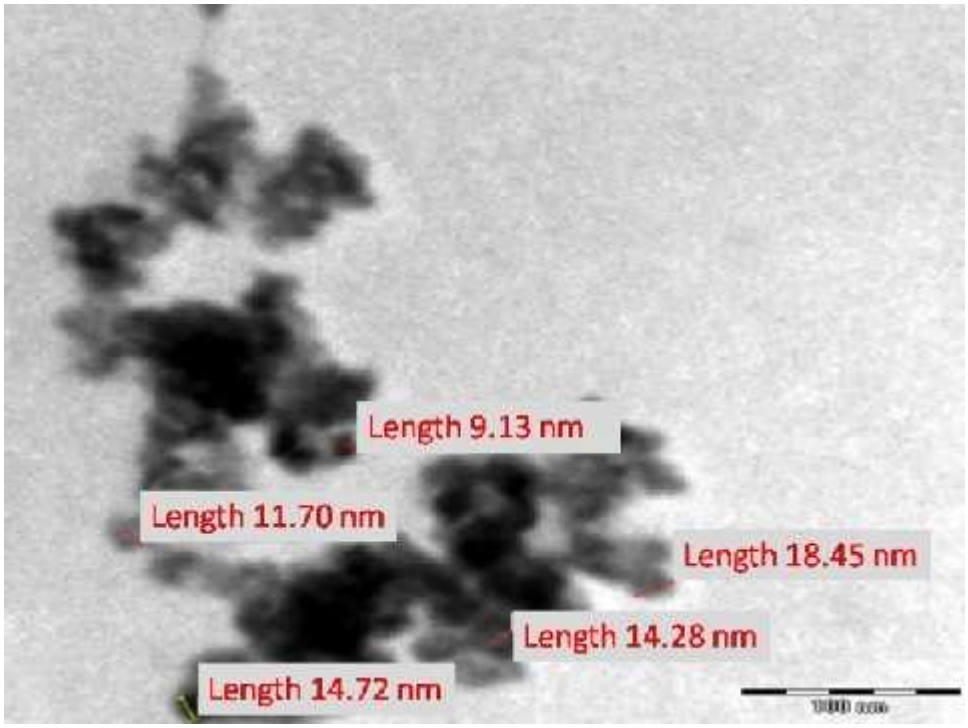

Sample 1A (0.075 M, calcined at 773 K)

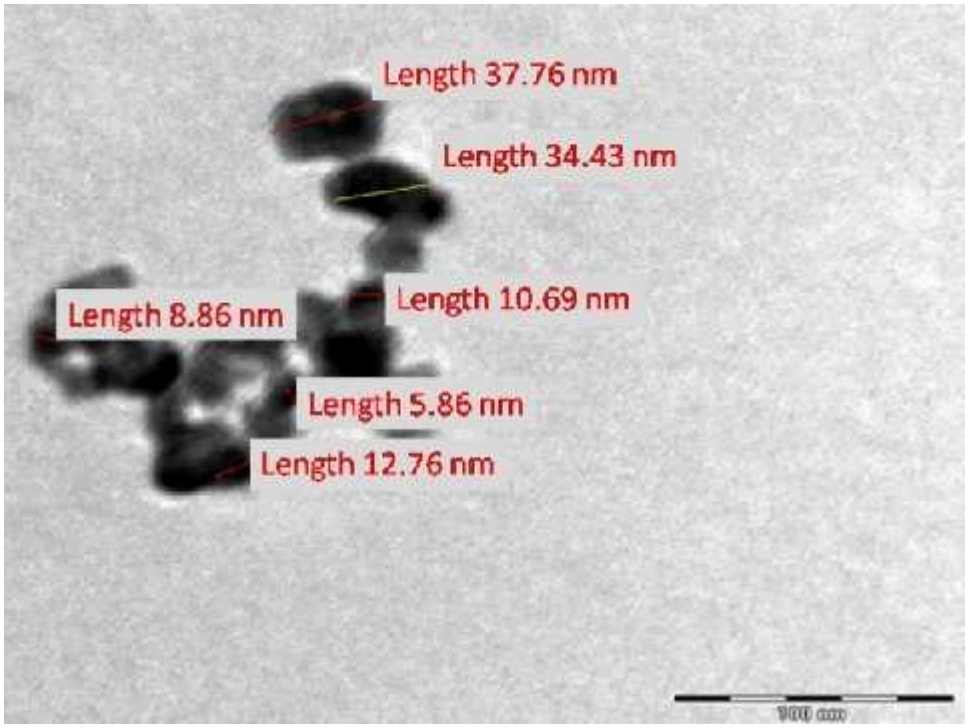

Sample 1B (0.075 M, calcined at 873K)

Figure 4.3 TEM of nano zirconia samples 1A and 1B

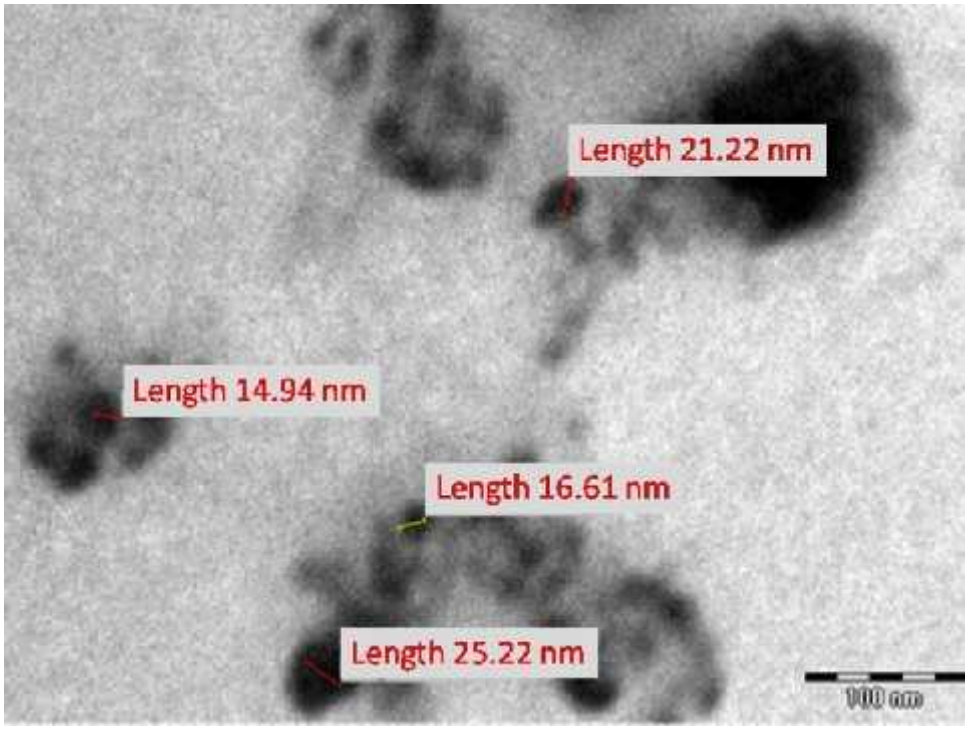

Sample 2A (0.05 M, calcined at 773 K)

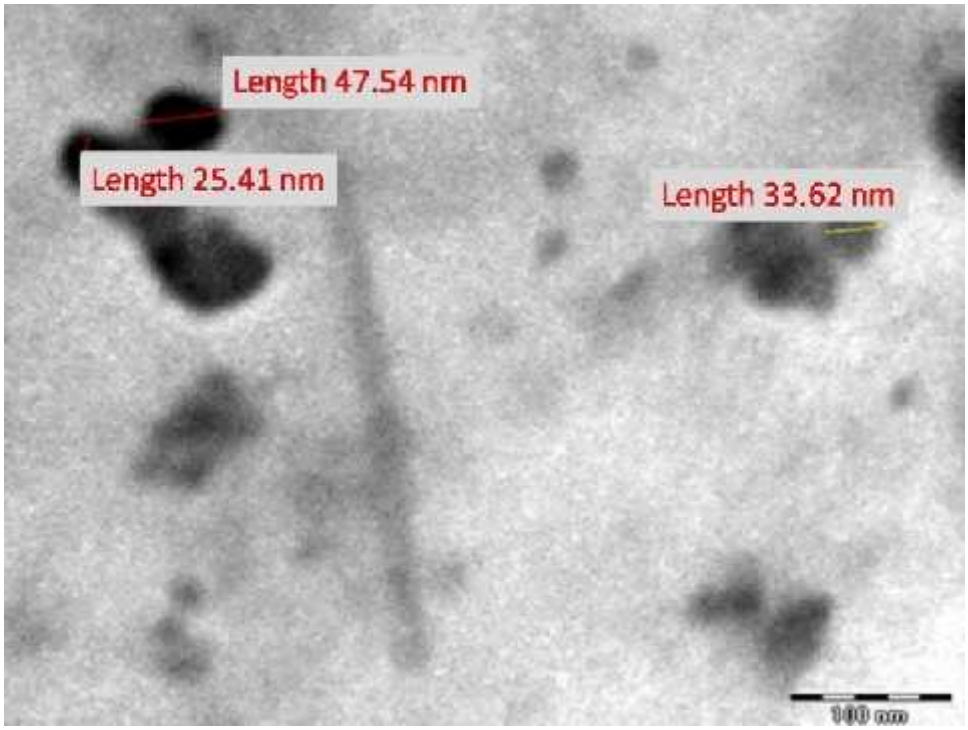

Sample 2B (0.05 M, calcined at 873K)

Figure 4.4 TEM of nano zirconia samples 2A and 2B

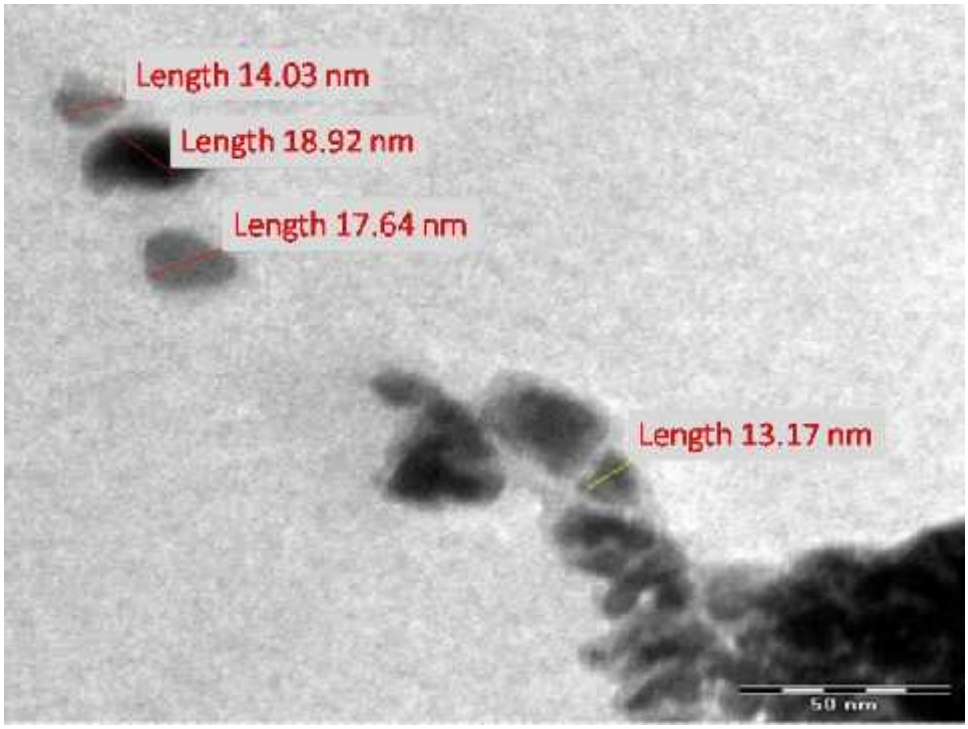

Sample 3A (0.025 M, calcined at 773 K)

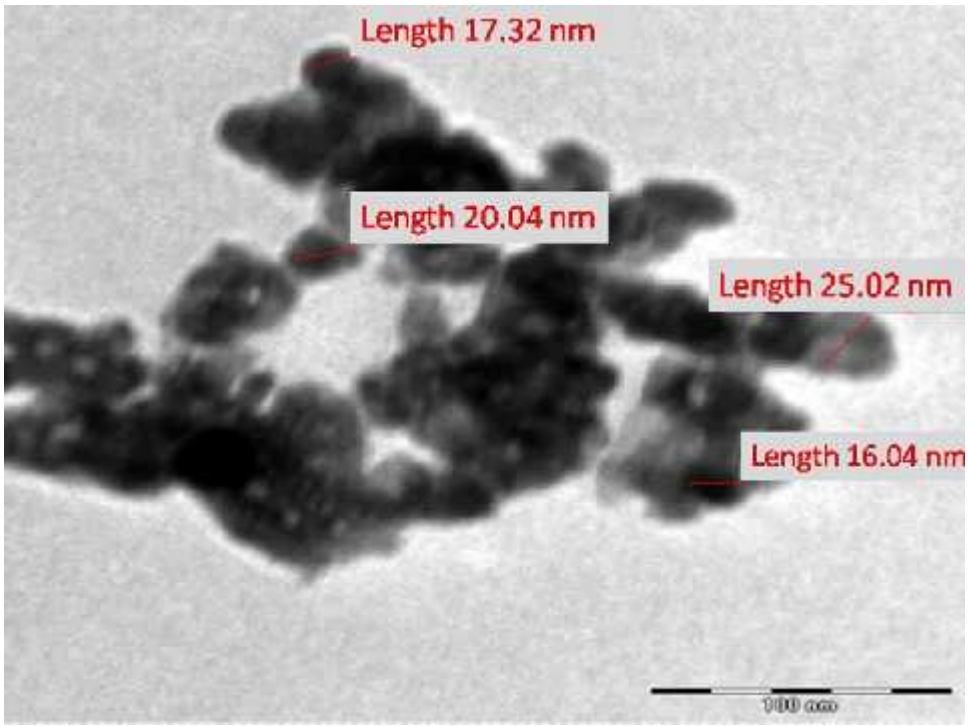

Sample 3B (0.025 M, calcined at 873K)

Figure 4.5 TEM of nano zirconia samples 2A and 2B

The reason for disparity of particle size calculated from TEM and XRD peak broadening is attributed to following basis (Dubey *et al.* 2016):

a) The variation of nano crystallite width and length in the TEM image are due to irregular shape of the nano crystals of various dimensions.

b) XRD analysis carried out for each of the crystallites present in the samples; however particle size analysis for TEM is carried out for few particles in the sample. However, TEM analysis to be more reliable than calculated values (Zhang *et al.* 2008).

4.6. DTA/TGA of nanocrystalline zirconia

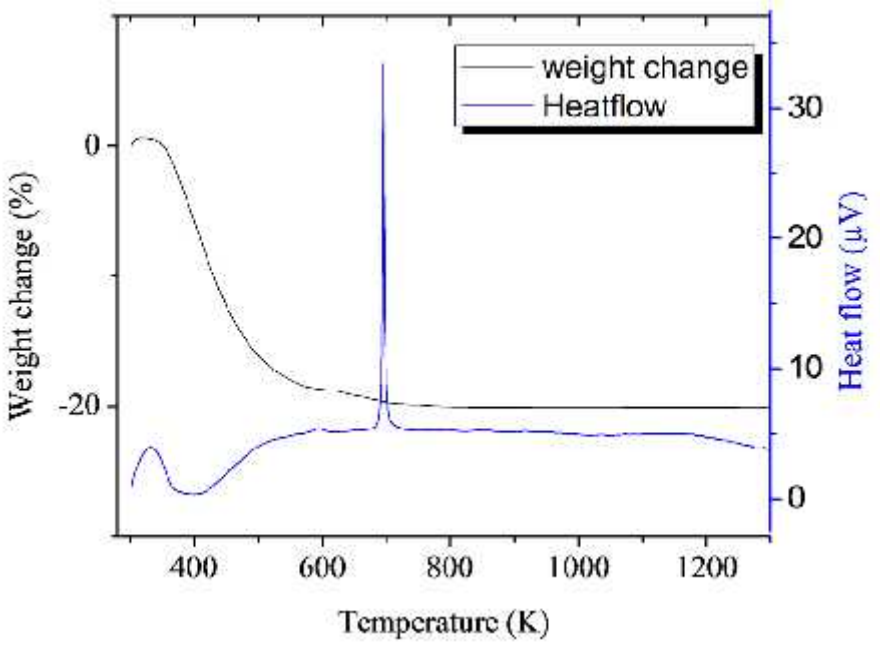

Figure 4.6 DTA /TGA of Zr $(OH)_4$ (0.075 M)

The TGA curve of all samples pursued similar trend (Figure 4.6), the weight of the sample declines with increase of temperature. There was a continous decline in weight in a temperature range of 323 K to 673 K. The mass loss in this temperature range is attributed to loss of water. Afterwards, the mass of the substance is stabilized. The loss of water happened together with broad endothermic peak at 389 K which is an indication of heat required to compensate the cooling due to evaporation of water.

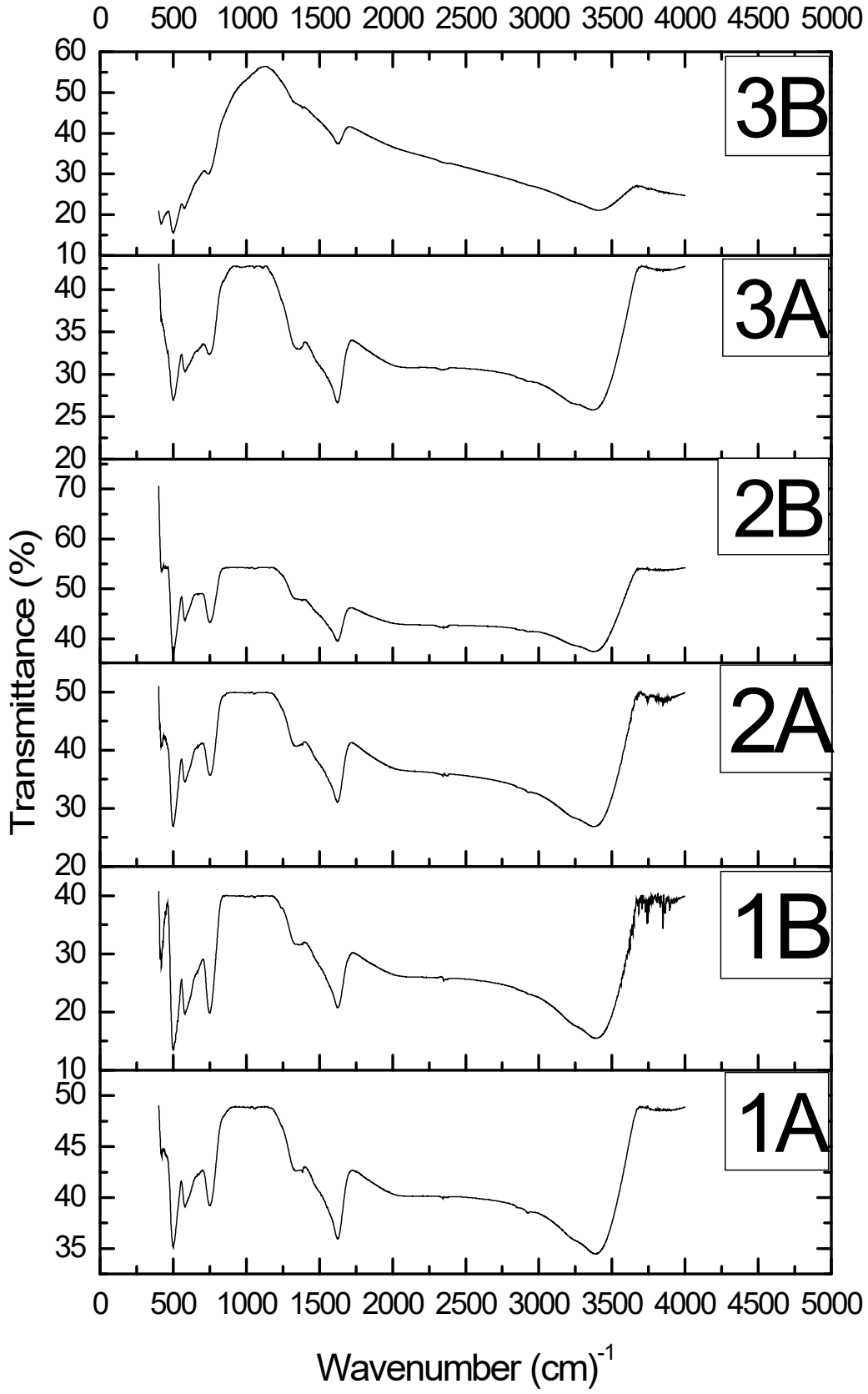

Figure 4.7 FTIR of synthesized nano zirconia samples

A small endothermic peak appeared at 573K, the peak is attributed to intialization of the crystallization of nano zirconia. The crystallization of nano zirconia is slow indicated by gradual loss of weight; it is attributed to slow release of bound hydroxyl bonds. At 695 K an exothermic peak was observed without any change in weight; this peak is attributed to the total crystallization of nano crystalline zirconia (Heshmatpour and Aghakhanpour 2011). The exothermic peak without any alteration in weight portrays the change of amorphous nano zirconia to crystalline zirconia (Heshmatpour and Aghakhanpour 2011). The lack of any exothermic peak following 695 K shows absence of amorphous zirconia above the temperature.

4.7. Fourier transform Infrared spectrocopy and surface area analysis of nanocrystalline zirconia

The FTIR of all samples are almost similar (Figure 4.7).The major characteristic peak of zirconia is present in the sample. The peaks at 740 and 500 cm^{-1} are attributed to Zr - O_2 - Zr asymmetric and stretching mode (Sahu and Rao 2000). The broad peak at 3400 cm^{-1} depicts stretching vibration of hydroxyl functional group OH (Deshmane and Adewuyi 2012). The peaks at 1600 cm^{-1} and 1380 cm^{-1} display bending vibrations of physioadsorbed water (Goharshadi and Hadadian 2012;Tyagi *et al.* 2006). The surface area and pore volume of nanocrystalline zirconia (sample 1A) were 24.17 m^2/g and 0.03025 cm^3/g respectively.

4.8. Synthesis of nano crystalline iron oxide/hydroxide

The adsorbent was synthesized by co-precipitation method. The reactions participating in the process of co-precipitation are as follows (Mascolo *et al.* 2013):

$$Fe^{3+} + 3OH^- \rightarrow Fe(OH)_3 \quad (4.4)$$

$$Fe(OH)_3 \rightarrow FeOOH + H2O \quad (4.5)$$

$$Fe^{2+} + 2OH^- \rightarrow Fe\,(OH)_2 \quad (4.6)$$

$$Fe\,(OH)_2 + 2Fe(OOH) \rightarrow Fe_3O_4 + 2\,H_2O \quad (4.7)$$

The ferrous and ferric hydroxides are precipitated. Afterwards, $Fe(OH)_3$ converted into FeOOH. The reaction between FeOOH and $Fe(OH)_2$ led to the formation of magnetite (Fe_3O_4).The magnetite (Fe_3O_4) synthesized is sensitive to oxidation and is partly oxidized to maghemite (Fe_2O_3) (Laurent *et al.* 2008).

4.9. XRD analysis of nano crystalline iron oxide/hydroxide

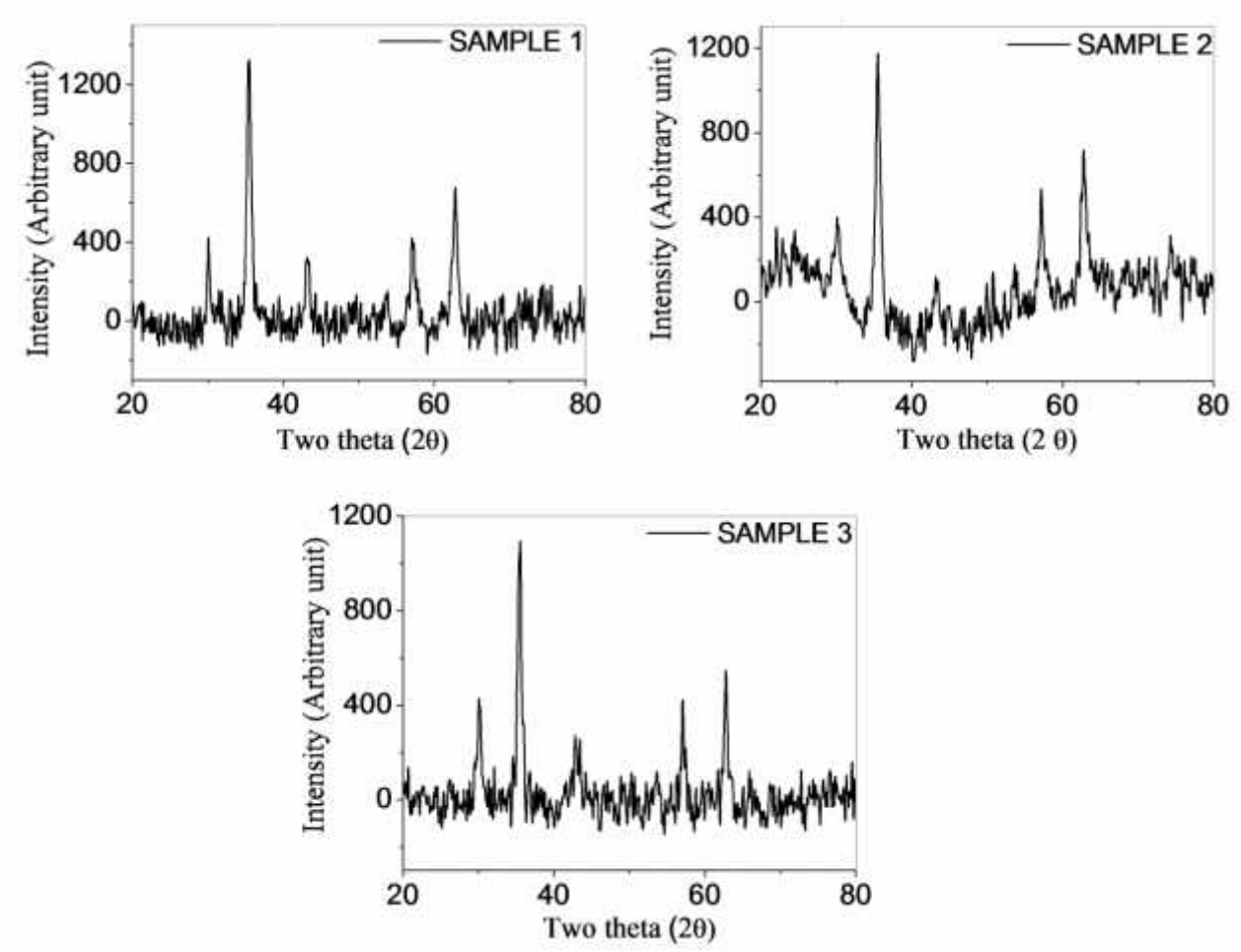

Figure 4.8 XRD diffractogram of nano crystalline iron oxide/hydroxide samples

The identification of material and its phases was investigated with the help of X-ray diffraction (Figure 4.8). The samples were scanned in the range of 20 – 80^o at the step rate of 0.4θ/s. In samples 1 and 3, magnetite phase is confirmed by major peaks occurring at ca. 35, 30 and 60 (JCPDS card no. 82- 1533) (ICDD 2003). However, maghemite phase also has same peak position (JCPDS card no. 39-1346) (ICDD 2003). In sample 2, one more peak appeared at position ca. 22 in addition to aforementioned peaks, it may be due to goethite (JCPDS-ICDD's card

no. 84-0464). The crystallite size (Table 4.3) was calculated by using Scherrer's equation (Equation 4.3)

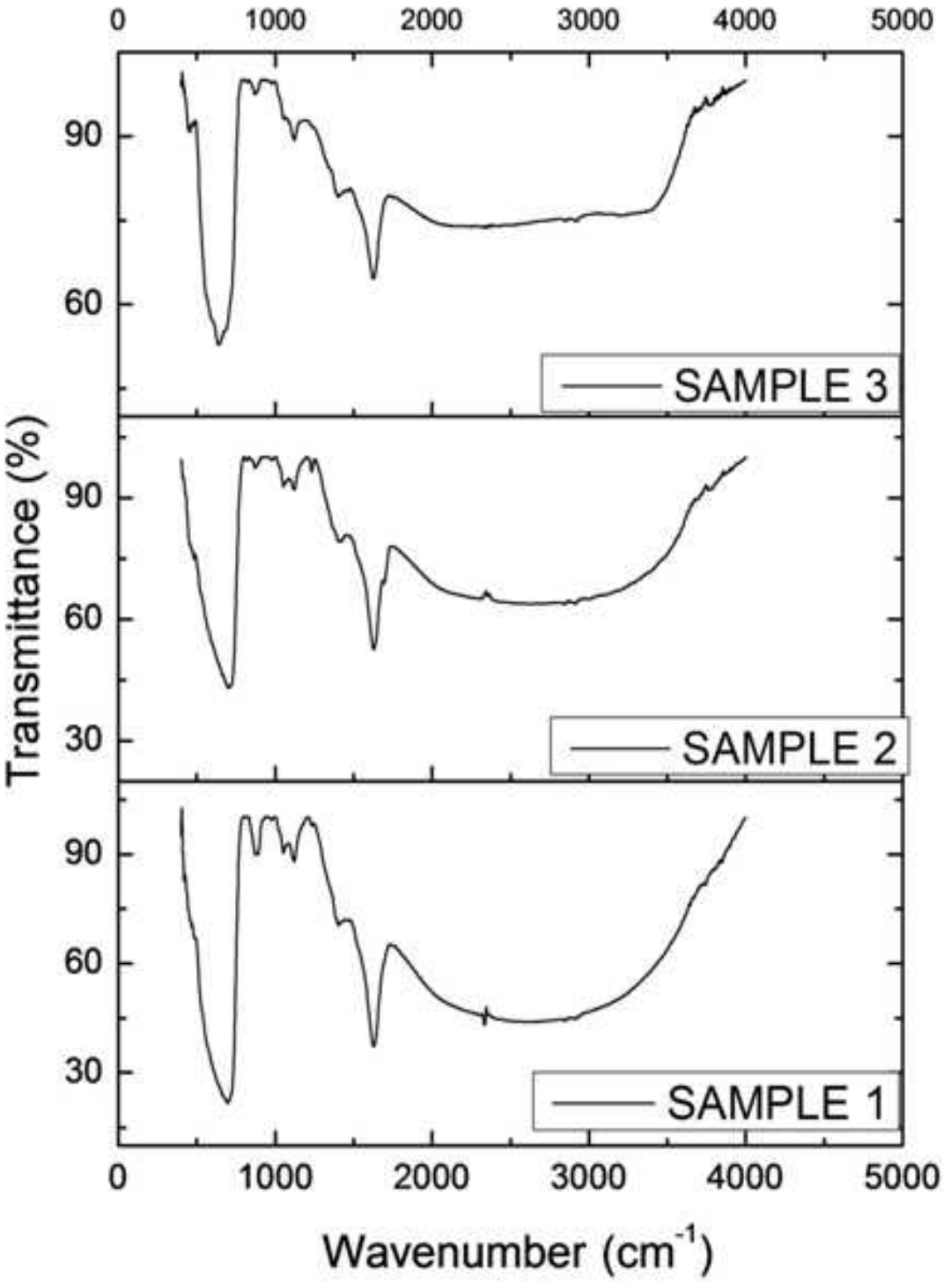

Figure 4.9 FTIR of nano crystalline iron oxide/ hydroxide samples

Table 4.3 XRD peaks and crystallite size of synthesized iron oxide/hydroxide

Sample 1		Sample 2		Sample 3	
2 θ (degree)	**Crystallite size (nm)**	**2 θ (degree)**	**Crystallite size (nm)**	**2θ (degree)**	**Crystallite size (nm)**
		22.12	26.66		
30.10	17.06	30.17	11.40	30.13	13.43
35.47	10.46	35.54	10.22	35.47	13.09
43.20	10.92	43.30	6.52	42.89	5.62
57.17	14.47	57.24	14.96	57.06	24.52
62.75	10.86	62.86	12.29	62.77	14.82

4.10. Fourier Transform Infrared Spectroscopy and surface area analysis of nano crystalline iron oxide/hydroxide

FTIR spectrum (Figure 4.9) of all materials conducted in the range 400 cm^{-1} to 4000 cm^{-1}. Fe-O bond is characterized by peak position at 700 cm^{-1} in FTIR spectrum. Peak at 881 cm^{-1} is due to FeO(OH). Peak at ca. 1600 cm^{-1} corresponded to physioadsorbed water (Cornell and Schwertmann 2006).The presence of maghemite and goethite is indicated by FTIR spectra. Thus, FTIR and XRD spectra confirmed the presence of maghemite and unreacted FeO(OH) (Iron oxide/ hydroxide) in the material. The surface area and pore volume of the nano crystalline iron oxide/hydroxide (sample 1) was 67.50 m^2/g and 0.1423 cm^3/g.

4.11. XPS and Magnetization studies of nano crystalline iron oxide/ hydroxide

XPS analysis (Figure 4.10) of all synthesized iron oxide/ hydroxide the samples for iron were carried out in the range of c.a 708 eV to ca. 730 eV. Peaks were fitted with the help of XPSPEAK41 software. Three peaks fitted at ca. 712, 720 and 725 are designated as peak 1, peak 2 and peak 3 respectively in Figure 4.10. Peak at ca. 712.49, 720.79 and 725.79 eV position were fitted for sample 1. Peaks at position 712.80, 720.67 and 726.70 eV fitted for sample 2 and 711.80, 720.06 and 725.40 for sample 3. The Fe^{3+} and Fe^{2+} $2p_{3/2}$ peaks reported in 710 to 711 eV range (Naumkin *et al.* 2016). Fe_2O_3 is characterized by satellite peak 8 eV higher

than the Fe $2p_{3/2}$ peak (Yamashita and Hayes 2008). In all samples, satellite peak is present. It confirmed the presence of Fe_2O_3. The $2p_{1/2}$ peak of Fe^{3+} and Fe^{2+} is present in all samples at 724ev.

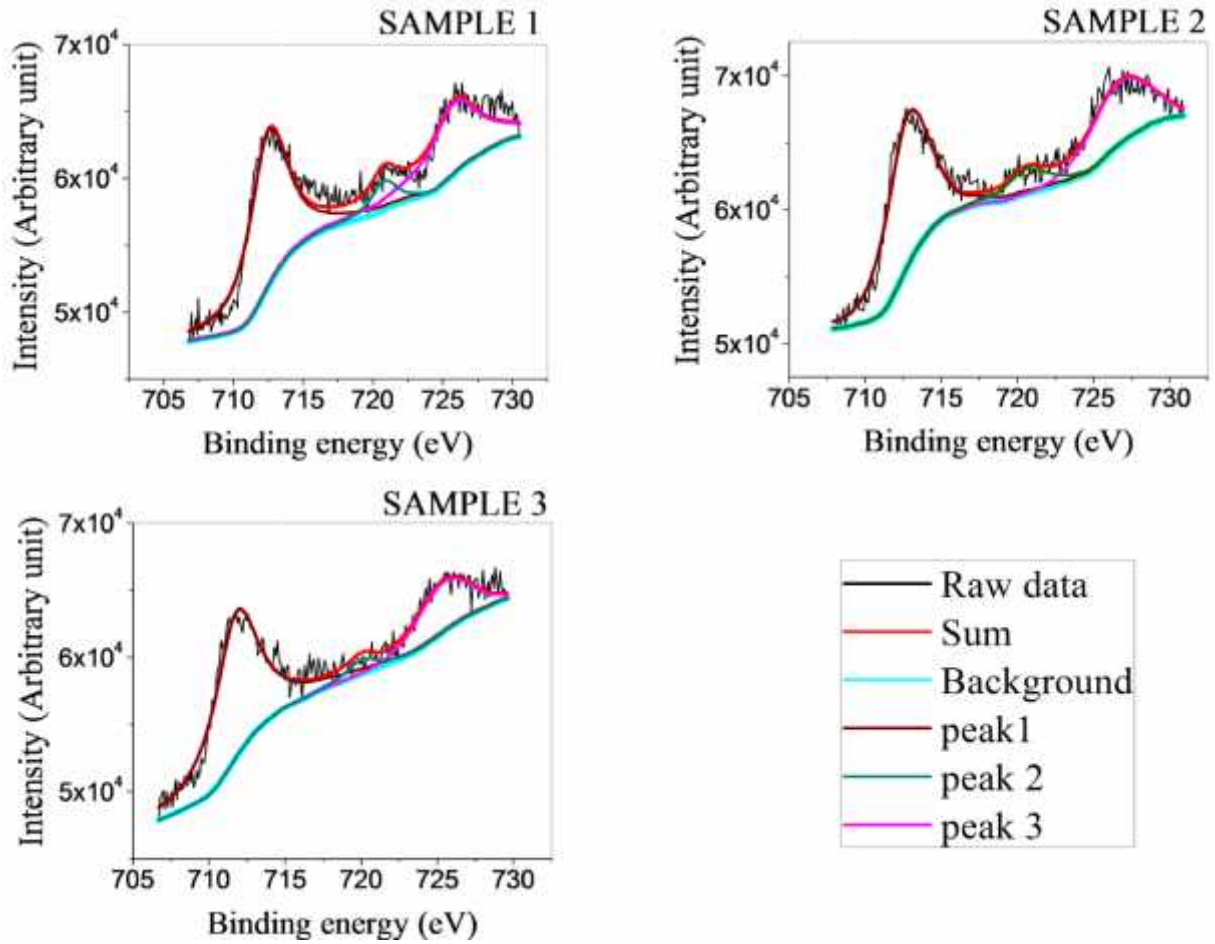

Figure 4.10 XPS of nano crystalline iron oxide/ hydroxide samples

M-H plot of the materials is presented in Figure 4.11. The analysis conducted from 3Tesla to -3 Tesla at 300K. Saturation magnetization was similar for all samples. Saturation magnetization was 69, 68 and 60 (emu/g) for samples 1, 2 and 3. A higher proportion of hematite and maghemite gives rise to low saturation magnetization of sample 3, as saturation magnetization of maghemite and hematite is lower than magnetite (Cao *et al.* 2008;Cornell and Schwertmann 2006).

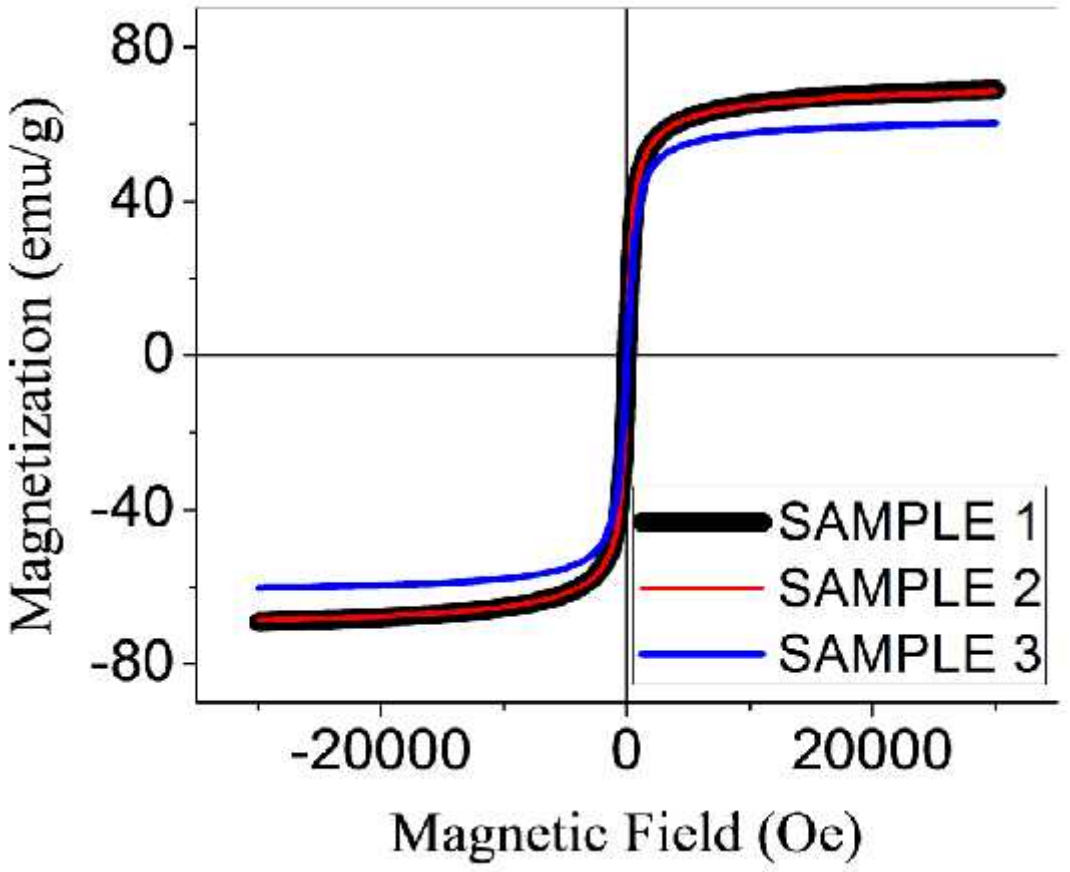

Figure 4.11 Magnetization curves of nano crystalline iron oxide/ hydroxide samples

4.12. Raman analysis of nano crystalline iron oxide/hydroxide

Raman analysis of the samples was carried out to investigate the different phases of iron oxide/hydroxide. Solid state laser of 532 nm wavelength is used for Raman analysis (Figure 4.12). Presence of Maghemite and Hematite is confirmed in all samples (Table 4.4). Sample 1 contains bands of goethite and magnetite, whereas sample 3 contains bands of magnetite in addition to maghemite and hematite. Hence, presence of Fe_2O_3 is supported by XPS analysis in all samples. In addition to this, magnetite peak is also present in the samples. Samples contain both Fe_3O_4 and Fe_2O_3 and in sample 1 there is presence of FeO(OH) also.

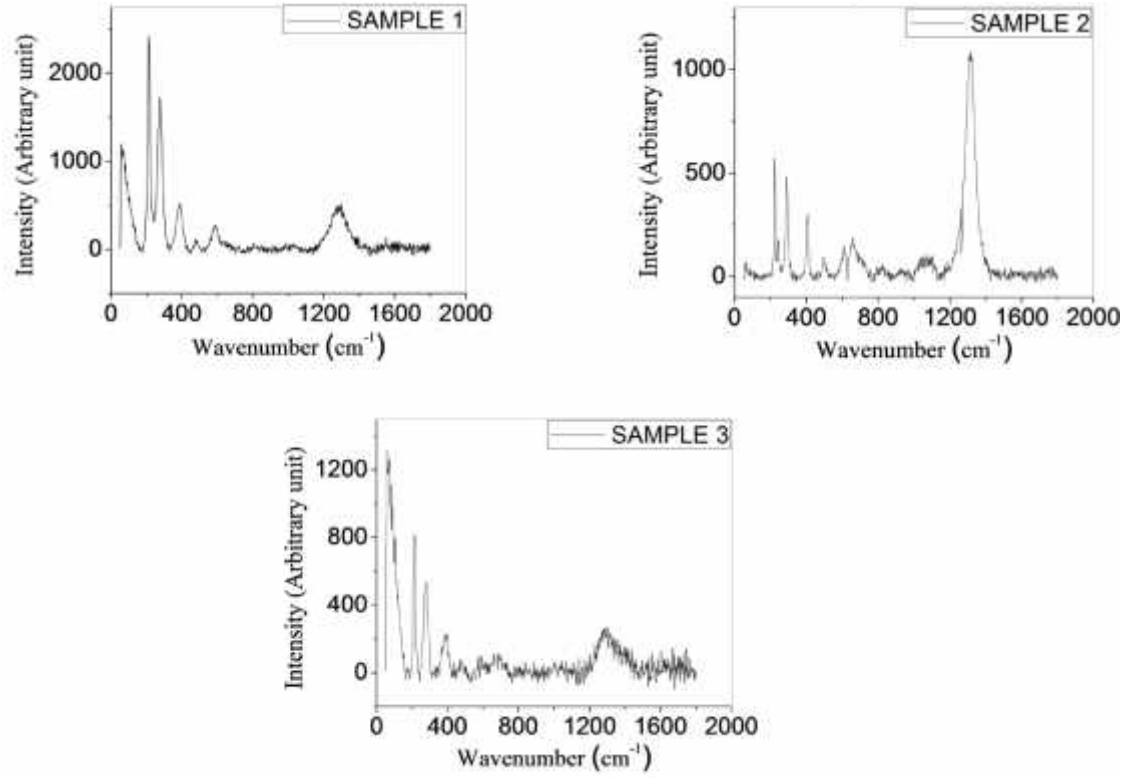

Figure 4.12 Raman spectrums of synthesized nano crystalline iron oxide/ hydroxide samples

Table 4.4 Observed Raman wavenumbers (cm^{-1}) of the synthesized iron oxide/ hydroxide sample

S.No	Sample 1	Sample 2	Sample 3	Assignment	Reference
1	57.63		57.66	Not assigned	
2	211.85		214.01	Magnetite	(Mitchell *et al.* 2015)
3		222.46		Hematite	(Legodi and de Waal 2007)
4		242.32		Hematite	(de Faria *et al.* 1997)
5	275.30		277.68	Magnetite	(Mitchell *et al.* 2015)
6		289.76		Hematite	(Legodi and de Waal 2007)
7	387.31		388.40	Maghemite	(Mitchell *et al.* 2015)
8		405.76		Hematite	(Umar *et al.* 2014)
9	474.84			Hematite	(Mitchell *et al.* 2015)
10		493.49		Hematite	(Sayed and Polshettiwar 2015)
11		607.70		Hematite	(Legodi and de Waal 2007)
12		655.38	675.62	Maghemite	(Legodi and de Waal 2007)
13	587.20			Goethite	(Legodi and de Waal 2007)
14	1283.61	1316.68	1271.69	Hematite	(de Faria *et al.* 1997)

4.13. SEM and TEM analysis of nano crystalline iron oxide/hydroxide

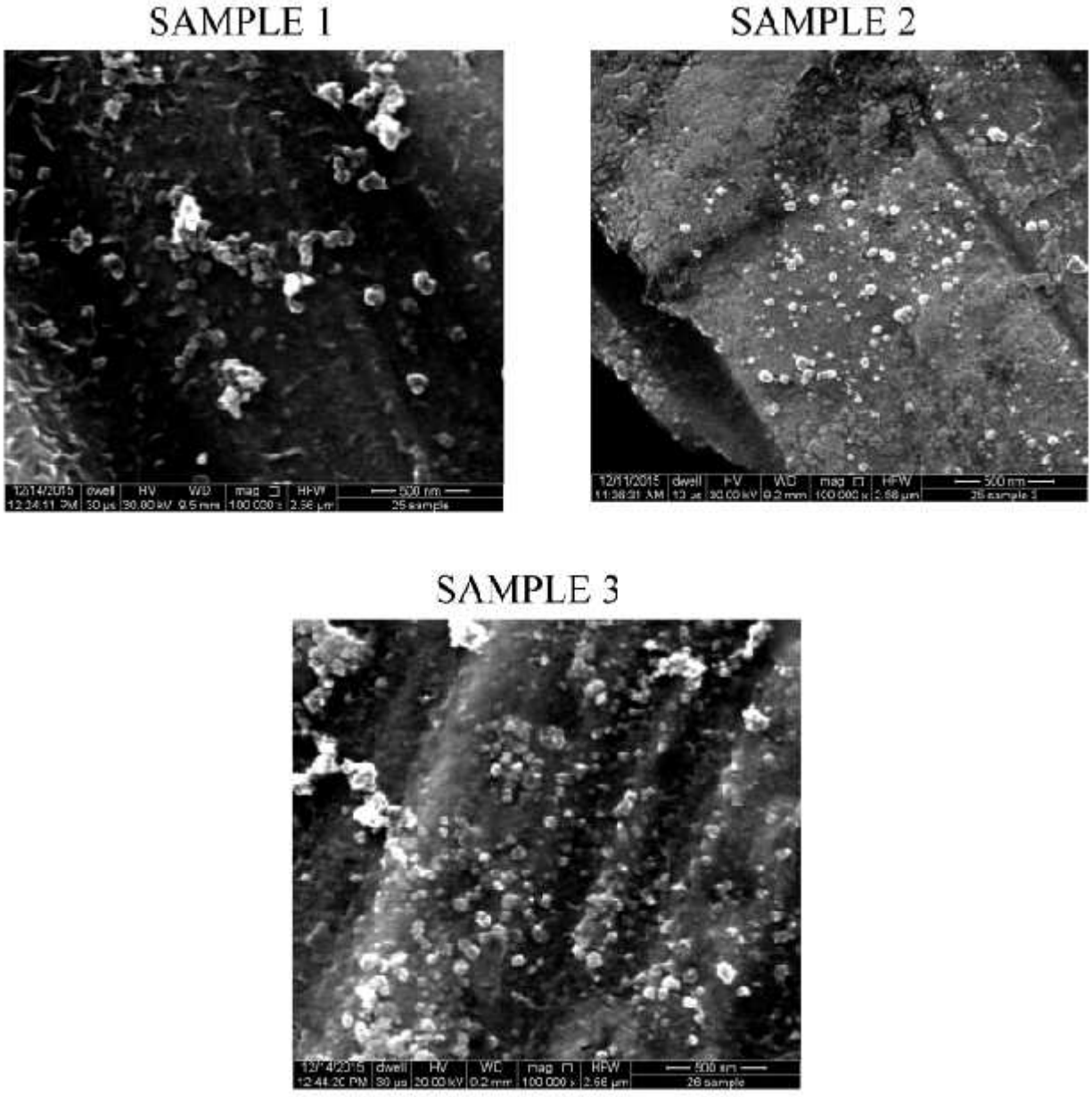

Figure 4.13 SEM images of iron oxide/ hydroxide

SEM analysis (Figure 4.13) of all samples was carried out to know the surface morphology. SEM images of all the samples were irregular and agglomerated. The particles were agglomerated due to absence of steric or electrostatic barriers (Misran *et al.* 2013). which could arise due to any co-solvents i.e. ethanol or methanol (Zhang *et al.* 1997). The barriers due to aforementioned reasons stabilize

the particles and prevented their agglomeration. However, in the present system, particles were agglomerated due to absence of such barriers.

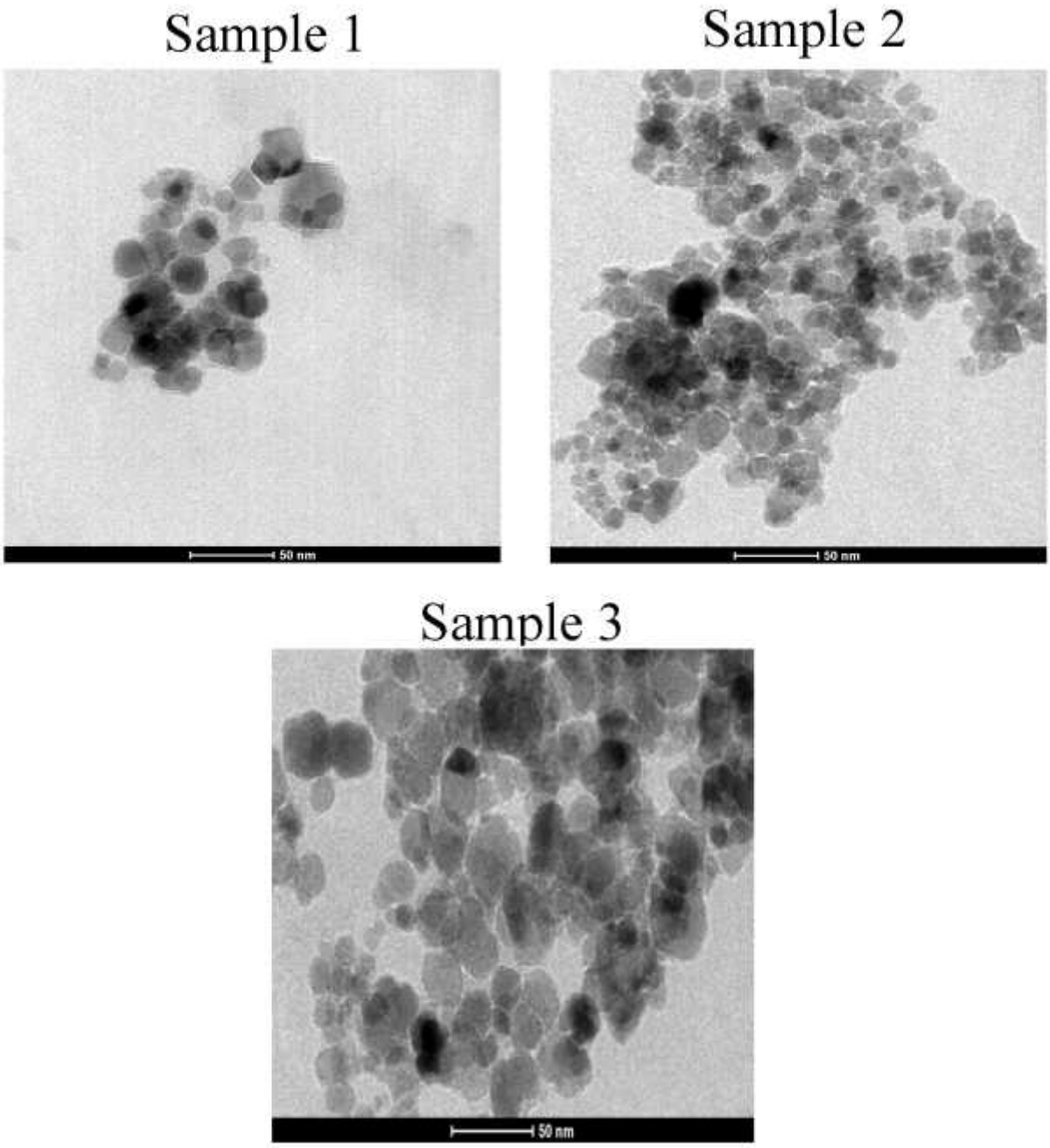

Figure 4.14 TEM images of iron oxide/ hydroxide

The particle size of the nano crystalline iron oxide/hydroxxide were determined with the help of TEM analysis (Figure 4.14). The shape of the particles was

irregular. The average particle sizes were 16, 12 and 18 nm for sample no 1, 2 and 3 repectively.The crystallite sizes calculated by XRD are in agreement with TEM particle size results.

4.14. Conclusions

Nano crystalline zirconia was synthesized. Crystallite size of nano zirconia rises with a raise of temperature except at peak position of 30 and 50 in sample 2 and sample 3. The particle size estimated from TEM analysis was more than the crystallite size estimated from XRD peak broadening. FTIR analysis shows the peak of Zr-O bond along with the peaks of physioadsorbed water. Nanocrystalline iron oxide/hydroxide (Fe_3O_4, Fe_2O_3 and trace quantity of FeOOH) was synthesized. XRD suggests the presence of Fe_3O_4 or Fe_2O_3. FTIR confirmed the presence of Fe-O bond. The XPS analysis confirmed the presence of Fe_2O_3 due to presence of satellite peak. Saturation magnetization was almost similar for all three samples. Raman analysis distinguished all phases of iron/oxide hydroxide in all samples and confirmed their presence. Particle size estimated by TEM analysis is in agreement with crystallite size estimated by XRD. SEM images of both the materials were agglomerated.